

# RSC Advances



This is an *Accepted Manuscript*, which has been through the Royal Society of Chemistry peer review process and has been accepted for publication.

*Accepted Manuscripts* are published online shortly after acceptance, before technical editing, formatting and proof reading. Using this free service, authors can make their results available to the community, in citable form, before we publish the edited article. This *Accepted Manuscript* will be replaced by the edited, formatted and paginated article as soon as this is available.

You can find more information about *Accepted Manuscripts* in the [Information for Authors](#).

Please note that technical editing may introduce minor changes to the text and/or graphics, which may alter content. The journal's standard [Terms & Conditions](#) and the [Ethical guidelines](#) still apply. In no event shall the Royal Society of Chemistry be held responsible for any errors or omissions in this *Accepted Manuscript* or any consequences arising from the use of any information it contains.



Journal Name

ARTICLE

## Preparation of polyetheretherketone composites with nanohydroxyapatite rods and carbon nanofibers having high strength, good biocompatibility and excellent thermal stability

Kai Wang Chan<sup>a</sup>, Cheng Zhu Liao<sup>b</sup>, Hoi Man Wong<sup>c</sup>, Kelvin Wai Kwok Yeung<sup>c</sup> and Sie Chin Tjong<sup>a\*</sup>

Received 00th January 20xx,  
Accepted 00th January 20xx

DOI: 10.1039/x0xx00000x

www.rsc.org/

Research into the development of polymeric materials for orthopedic implants is becoming ever more important since the demand of biocompatible implants steadily increases in recent years globally. Bioinert polyetheretherketone (PEEK) is typically reinforced with bioactive hydroxyapatite microparticles. However, the tensile strength of conventional PEEK/hydroxyapatite microcomposites falls sharply with increasing filler loading. To address low strength and high filler loading issues, nanohydroxyapatite rods (nHA) and carbon nanofiber (CNF) were employed to reinforce PEEK. In this study, molded-grade PEEK pellets, nHA and CNF fillers were melt-mixed and injection molded to form PEEK/nHA and hybrid PEEK/nHA-CNF nanocomposites. The tensile and thermal properties, as well as bioactivity and biocompatibility of such nanocomposites were investigated. Tensile tests results showed that elastic modulus of PEEK/nHA nanocomposites increases with increasing nHA content. The PEEK/9.3vol% nHA nanocomposite exhibited higher tensile strength than conventional HAPEX microcomposite. Thermogravimetric measurements indicated that the nHA addition improves thermal stability of PEEK. Thus PEEK/9.3vol% nHA nanocomposite with good mechanical, thermal and biological performances was an attractive biomaterial for use in maxillofacial surgery. Furthermore, the tensile property of PEEK/15vol% nHA-1.9vol%CNF nanocomposite was compared favorably with that of human cortical bones. The results of biomineralization, alkaline phosphatase (ALP), 3-(4,5-dimethylthiazol-2-yl)-2,5-diphenyltetrazolium bromide (MTT) and 2-(4-iodophenyl)-3-(4-nitrophenyl)-5-(2,4-disulfophenyl)-2H-tetrazolium (WST-1) assays also showed that the PEEK/15vol% nHA and PEEK/15vol%nHA-1.9vol% CNF nanocomposites exhibit excellent bioactivity and biocompatibility. ALP assay showed good activity of osteoblast cells on the composite specimens with high nHA content. Moreover, CNF addition further increased ALP activity of PEEK/15vol% nHA nanocomposites. The PEEK/15vol% nHA-1.9vol% CNF composite with enhanced tensile strength and excellent biocompatibility shows large potential for load-bearing implant applications.

### Introduction

In recent years, there is a substantial increase in the number of accidents in the workplace, road traffic and sport activity. These result in unavoidable bone injuries. Furthermore, the number of aging population also increases dramatically in developed and undeveloped countries.<sup>1,2</sup> Elderly people have a higher risk of

<sup>a</sup>Department of Physics and Materials Science, City University of Hong Kong, Tat Chee Avenue, Kowloon, Hong Kong

<sup>b</sup>Department of Materials Science and Engineering, South University of Science and Technology of China, Shenzhen, China

<sup>c</sup>Department of Orthopedics and Traumatology, Li Ka Shing Faculty of Medicine, The University of Hong Kong, Hong Kong

\*Corresponding Author

bone fracture that imposes significant social and economic burdens to our society. Autografts removed from the bones of patients and allografts taken from cadavers are traditionally used for replacing bone tissue defects. Both autografts and allografts have many drawbacks including limited availability, immunological rejection and possible disease transmission.<sup>3</sup> Therefore, there is a high demand for artificial implants with excellent biocompatibility in orthopedics. Metallic alloys are widely used for making bone fixation devices and implants. Metallic alloys offer beneficial advantages such as high mechanical flexibility due to their superior ductility and toughness.<sup>4</sup>

Metallic materials like stainless steels, Co-Cr and Ti-6Al-4V alloys have been used extensively for fabricating load-bearing hip implants. However, these implants undergo corrosion upon exposure to human body fluid. Released ions from the implants can cause allergy, inflammation and cytotoxicity.<sup>5-9</sup> The presence of 0.9% NaCl in body fluid can also induce pitting. The chloride ion attacks protective passive films formed on metallic surfaces.<sup>10,11</sup> The movement of an artificial hip prostheses produces metallic wear debris that can lead to the secretion of cytokines by macrophages.<sup>12</sup> These cytokines then recruit more immune cells to the site of inflammation and form giant cells.<sup>13</sup> Metallic implants also experience stress shielding effect due to their elastic modulus far exceeds that of cortical bones.

Polymers are attractive materials for fabricating bone implants because of their good processability and light weight.<sup>14-19</sup> Polyetheretherketone (PEEK) exhibits high melting temperature (343 °C), high temperature durability, excellent radiation stability and high Young's modulus (3.8 GPa).<sup>20</sup> Accordingly, PEEK has been increasingly used for making trauma, orthopedic and spinal fixation devices.<sup>21-23</sup> From a review study on recent biomedical applications of PEEK and its composites reinforced with carbon fibers (CFs), PEEK is currently used for fabricating cervical spine cage and lumbar spinal fusion while PEEK/CF composites are employed for acetabular cup, bearing components in hip and knee implants.<sup>24</sup> In addition, PEEK has also found application for making custom made implants for craniofacial surgery recently.<sup>25</sup> PEEK is bioinert, thus it inhibits protein adsorption and cell adhesion.<sup>26,27</sup> Its biocompatibility can be improved either via surface modification<sup>28,29</sup> or by adding bioactive hydroxyapatite (HA) fillers in the form of whiskers and particulates.<sup>30-34</sup> Abu Bakar et al. incorporated large HA microparticulates (mHA) into PEEK.<sup>32,33</sup> They reported that the tensile modulus of

the composites increases while the tensile strength decreases with increasing filler content. Poor interfacial bonding causes decohesion of mHA particles from the PEEK matrix.

Generally, large HA particulates often fracture into small fragments during tensile loading. Large filler loading levels often lead to poor processability of polymercomposites.<sup>34-38</sup> Recent development in nanotechnology allows scientists to synthesize various nanomaterials with enhanced chemical, physical and mechanical properties.<sup>39-41</sup> In particular, ceramic nanomaterials with excellent biocompatibility show large potential for use in biomedical sectors.<sup>42-50</sup> Nanotechnology opens new opportunities for developing novel biomaterials that can mimic and reinforce bone tissues.<sup>51-53</sup> Furthermore, only low loading levels of nanofillers are needed for reinforcing polymers.<sup>54-57</sup>

Bone tissue is a biocomposite consisting of a collagen matrix and HA nanorods (nHA) in which cortical bone having an elastic modulus of 7 GPa.<sup>58</sup> Synthetic nHA promotes protein adsorption and osteoblast growth, leading to osseointegration.<sup>45</sup> Therefore, nHA/polymer composites have been studied for their clinical use in load-bearing hip prostheses and bone tissue engineering recently.<sup>59-62</sup> In previous study, we have prepared PEEK composites using nHA and PEEK powders via powder processing and furnace sintering.<sup>59</sup> In the process, both nHA and PEEK powders are first mechanically mixed followed by furnace sintering. However, powder processing technique is inadequate to make PEEK nanocomposites with optimal mechanical properties. It requires high filler loading, i.e. 50 wt % nHA (29.2 vol% nHA) to achieve an elastic modulus of 6.73 GPa.<sup>59</sup> Recently, Wang et al. fabricated PEEK/nHA nanocomposites by mechanical mixing PEEK powders with nHA rods followed by injection molding.<sup>63</sup> They reported that the fracture strength of all nanocomposites is poorer than that of pure PEEK. The poor performance of such PEEK/nHA composites resulted from the use of PEEK powders. In this study, we intend to employ nHA and molded-grade PEEK pellets to fabricate PEEK/nHA biocomposites using injection molding. To further enhance mechanical performance of PEEK/nHA nanocomposites, carbon nanofibers (CNFs) are simultaneously added to the PEEK/nHA composites. Carbon nanofibers generally exhibit good biocompatibility<sup>64,65</sup>, and are very effective for reinforcing PEEK.<sup>66</sup> Thus it is feasible to produce biocompatible PEEK/nHA-CNF composites with good mechanical properties commercially in bulk quantities using injection molding process.

## Experimental

### Materials

Nanohydroxyapatite rods were purchased from Nanjing Emperor Nanomaterial (China). Transmission electron microscopy (TEM; Philips CM20) image of nHAs was shown in Fig. 1. PEEK-Optima pellets and carbon nanofibers were bought from Invibio Company and Nanostructured & Amorphous Materials Inc. (USA), respectively. Inorganic reagents such as CaCl<sub>2</sub>, NaCl, KCl, KH<sub>2</sub>PO<sub>4</sub>, NaHPO<sub>4</sub>, NaHCO<sub>3</sub> and Na<sub>2</sub>SO<sub>4</sub> were supplied by Sigma-Aldrich Inc. (U.S.A.). They were used directly without further purification. PEEK pellets and nHA were dried in an oven at 55 °C overnight prior to melt-compounding.

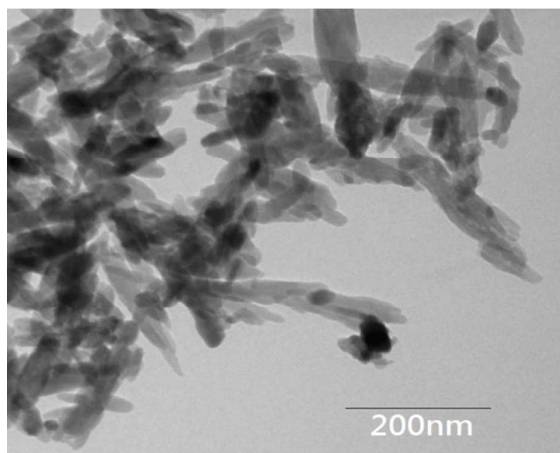


**Figure 1.** TEM micrograph of HA nanorods

### Preparation of nanocomposites

The chemical compositions of binary nHA/PEEK nanocomposites were listed in Table 1. Carbon nanofibers were only added to nHA/PEEK composites with high filler contents to create hybrid composites. The compositions of all composite samples in this article were expressed in volume percentage. Dried PEEK pellets and nHA were initially compounded in a Brabender at a screw rotation speed of 30 rpm for 45 min. The mixing temperatures of Brabender from hopper to extrusion die were kept at 360-380-390-395-380-360°C, respectively. The extrudates were cut into small pellets by a pelletizer and fed into Brabender

again for second mixing under the same conditions to achieve homogeneous dispersion of nanofillers in the polymer matrix. The extruded products were pelletized again, dried overnight in an oven and finally fed into an injection molder (Toyo TI-50H) to produce dog-bone tensile bars and circular disks. The disks were mainly used for cell culture, cell viability and alkaline phosphatase activity measurements.

**Table 1.** The compositions of PEEK/nHA and PEEK/nHA-CNF nanocomposites

Specimens	nHA		CNF	
	wt%	vol%	wt%	vol%
PEEK	0	0	0	0
PEEK/4.4vol% nHA	10	4.4	0	0
PEEK/9.3vol% nHA	20	9.3	0	0
PEEK/15vol% nHA	30	15	0	0
PEEK/21.5vol% nHA	40	21.5	0	0
PEEK/9.3vol % nHA- 1.6vol% CNF	20	9.3	2	1.6
PEEK/15vol% nHA- 1.9vol% CNF	30	15	2	1.9

### Material characterization and tensile tests

The morphological features of as-fabricated composite specimens, and osteoblasts adhered on specimen surfaces were examined in a SEM (Jeol JSM 820). The composites were dipped in liquid nitrogen and then fractured by a hammer. The fractured surfaces were then coated with a thin carbon film. Tensile tests were performed at room temperature using an Instron tester (model 5567) at a crosshead speed of 1 mm min<sup>-1</sup>. The elastic modulus of PEEK-based composites was determined from the linear region of stress-strain curves. Five samples of each composition were tested, and the average values were reported.

### Thermogravimetric Analysis

Thermogravimetric experiments were carried out using the TGA1 STARe system (Mettler Toledo AG, Switzerland) in a nitrogen atmosphere from 50 to 800 °C at 10°C/min. The temperatures at 10% weight loss

( $T_{10\%}$ ) and 30% weight loss ( $T_{30\%}$ ) were determined from the weight loss vs temperature curves.

### Cell culture

Human osteoblasts (Saos-2) were cultured in Dulbecco's Modified Eagle's Medium (DMEM) supplemented with 10% fetal bovine serum, penicillin and streptomycin. Injection molded disks were sliced into small rectangles for cell seeding and growth measurements. These samples were ground with SiC papers of different grades, followed by rinsing with 70% ethanol and phosphate buffer saline (PBS) solutions. Rinsed samples were placed in a 96-well plate; a cell suspension was pipetted at  $10^4$  cells per well. The plate was placed inside an incubator under a humidified atmosphere of 5% CO<sub>2</sub>/95% air at 37 °C for 1 and 3 days, respectively. The culture medium was changed every two days. Following the incubation, the samples were washed with phosphate-buffered saline (PBS), fixed with 10% formaldehyde, dehydrated in a graded series of ethanol. Dehydrated cells were critical point dried, sputter deposited with gold in preparation for SEM examination.

### Cell viability

Osteoblastic cell viability was assessed using 3-(4,5-dimethylthiazol-2-yl)-2,5-diphenyltetrazolium bromide (MTT), and 2-(4-iodophenyl)-3-(4-nitrophenyl)-5-(2,4-disulfophenyl)-2H-tetrazolium (WST-1) assays. A suspension with  $10^4$  cells was seeded in each well (96-well plate) containing test samples (number of specimens,  $n = 5$ ). The plate was incubated in a humidified atmosphere of 5% carbon dioxide in air at 37 °C for 3, 7 and 10 days, respectively. The culture medium was refreshed every 3 days. At days 3, 7 or 10, the medium was aspirated, then 10  $\mu$ L of MTT solution (5mg MTT: 1 mL DMEM) was added to each well and incubated for 4h at 37 °C. In the process, tetrazolium ring of MTT salt was cleaved by mitochondrial enzyme, i.e. succinic dehydrogenase of viable osteoblasts, forming insoluble formazan crystals. MTT formazan was insoluble in water, thus an organic solvent was needed to solubilize the crystals. The formazan was dissolved in 10% sodium dodecyl sulfate (SDS)/0.01 M hydrochloric acid (100  $\mu$ L). The absorbance of dissolved formazan was measured at a wavelength of 570 nm using a multimode detector (Beckman Coulter DTX

880), with a reference wavelength of 640 nm. The results were expressed in terms of mean  $\pm$  standard deviation (SD). MTT tests were repeated at least twice.

For WST-1 assay, the samples ( $n \geq 3$ ) were first cultured with osteoblasts °C for 3, 7 and 10 days, respectively. After cell culturing for every prescribed time period, tetrazolium salt was added to each well followed by incubation for 4h at 37 °C. Cleavage tetrazolium product was water soluble, thus eliminating solubilization step as required for the MTT assay. The amount of formazan formed was directly proportional to the number of metabolically active cells in the culture. The amount of water-soluble formazan was quantified by the absorbance at 450 nm. WST-1 tests were repeated at least twice. Statistical significance was assessed by the Student t-test, with a significance level of  $p < 0.05$  as compared to pure PEEK.

### Alkaline phosphatase activity

Alkaline phosphatase (ALP) is an enzyme secreted by osteoblasts during osteogenesis and acts as the marker for their differentiation. The ALP activity of each sample (number of specimens,  $n = 5$ ) was assessed by a colorimetric assay kit (No 2900-500, Stanbio Laboratory, Boerne, Texas) according to the manufacturer's instructions. The kit employed colorless 4-nitrophenyl phosphate as a substrate. The enzyme ALP of the cells hydrolyzed the substrate to color 4-nitrophenol and an inorganic phosphate. In the measurements, test samples were placed in each well of a 24-well plate. Osteoblasts were cultured on the samples for 3, 7 and 14 days. The culture medium was changed every 3 days. At selected days 3, 7 or 14, the cells were rinsed with PBS, and lysed with 0.1% triton X-100 at 4 °C for 30 min. The cell lysates were then centrifuged at 4 °C followed by placing 10  $\mu$ L of the supernatant of each sample in a 96-well plate. Finally, p-nitrophenyl phosphate was added to the plate. The absorbance of p-nitrophenol formed was measured using a spectrophotometer (Beckman Coulter DTX 880) at 405 nm. The rate at which p-nitrophenol formed was directly proportional to ALP activity. The ALP activity was normalized to DNA content of the samples. DNA standard (Calf thymus DNA, Ultrapure D-4764; Sigma Aldrich) and Hoechst 33258 dye (Sigma Aldrich) were used in the tests. Hoechst 33258 nucleic acid dye

emitted blue fluorescence at 465 nm when bound to double-stranded DNA.

### Biom mineralization test

The PEEK-based nanocomposites were immersed in a simulated body fluid (SBF) solution at 37 °C for 21 days for assessing their bioactivity. This solution was prepared according to the corrected Kokubo protocol by dissolving required amounts of reagent grade chemicals including NaCl, NaHCO<sub>3</sub>, KCl, K<sub>2</sub>HPO<sub>4</sub>·3H<sub>2</sub>O, MgCl<sub>2</sub>·6H<sub>2</sub>O, CaCl<sub>2</sub>·2H<sub>2</sub>O and Na<sub>2</sub>SO<sub>4</sub> into distilled water to give desired ion concentrations: Na<sup>+</sup> (142 mM), K<sup>+</sup> (5 mM), Ca<sup>2+</sup> (2.5 mM), Mg<sup>2+</sup> (1.5 mM), Cl<sup>-</sup> (147.8 mM), HCO<sub>3</sub><sup>-</sup> (4.2 mM), HPO<sub>4</sub><sup>-</sup> (1 mM) and SO<sub>4</sub><sup>2-</sup> (0.5 mM). The pH value of solution was adjusted to 7.4 using tris-(hydroxymethyl)-aminomethane and 1M HCl at 37 °C.<sup>67,68</sup> After immersion, the specimens were removed from the solution, rinsed with distilled water, dried, and then examined in SEM as well as X-ray diffractometer (XRD; Bruker, USA) under CuK $\alpha$  radiation at 30 kV.

## Results and discussion

### Morphology

Figure 2a shows the SEM image of PEEK/4.4 vol% nHA nanocomposite. It can be seen that the nHA fillers are dispersed uniformly in the polymer matrix. The polymer matrix is quite ductile as characterized by the presence of rough surface. By increasing nHA content to 15 vol%, most nHA fillers are still dispersed homogeneously, but few nHA fillers tend to aggregate to form small agglomerates. For the PEEK/15 vol% nHA-1.9vol% CNF composite, CNF fillers can be readily seen (Fig. 2b). As recognized, polymer nanocomposites are generally reinforced with very low loading levels of fillers (e.g. 0.2 - 2 vol %) to achieve desired chemical, physical or mechanical properties. However, polymer nanocomposites for bone implant applications require the additions of higher nHA loadings because the polymeric matrix is bioinert. Such nHA fillers can anchor osteoblasts and promote their growth on the surfaces of polymer nanocomposites. It should be noted that the nHA filler contents of PEEK/nHA nanocomposites are much lower than the mHA loadings in conventional PEEK/mHA microcomposites.

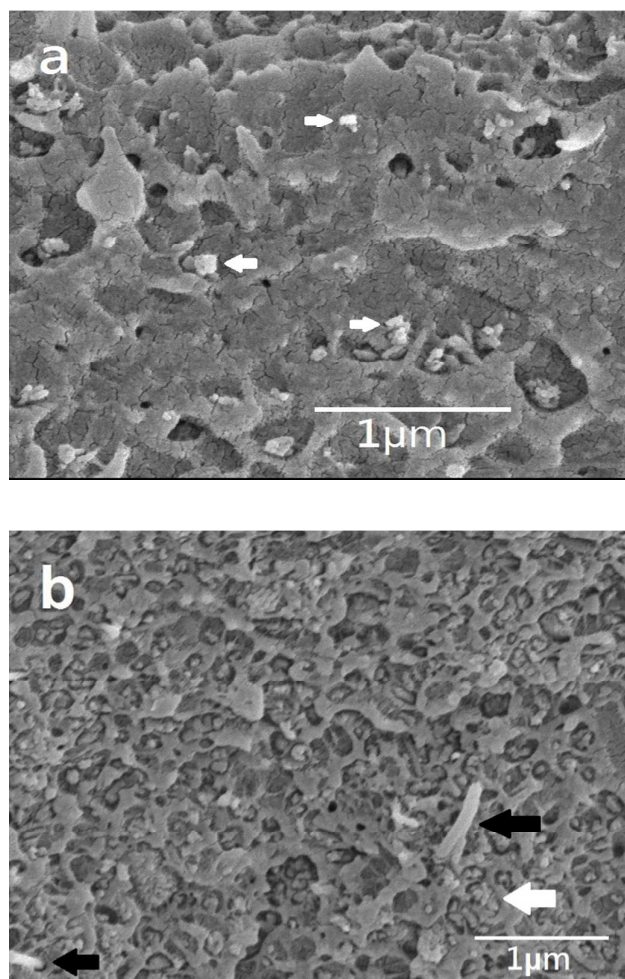
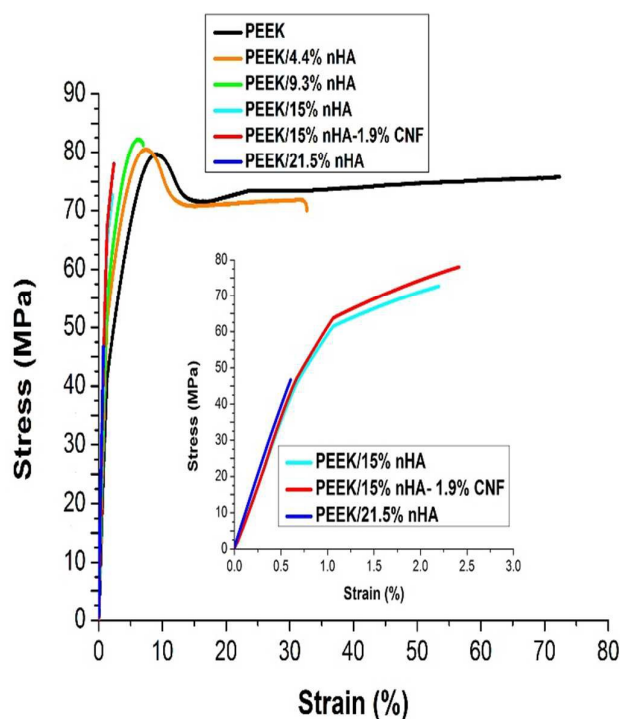


Figure 2. SEM micrographs showing fracture surfaces of (a) PEEK/4.4% nHA and (b) PEEK/15% nHA-1.9% CNF nanocomposites. Black arrow: CNF; white arrow: nHA.

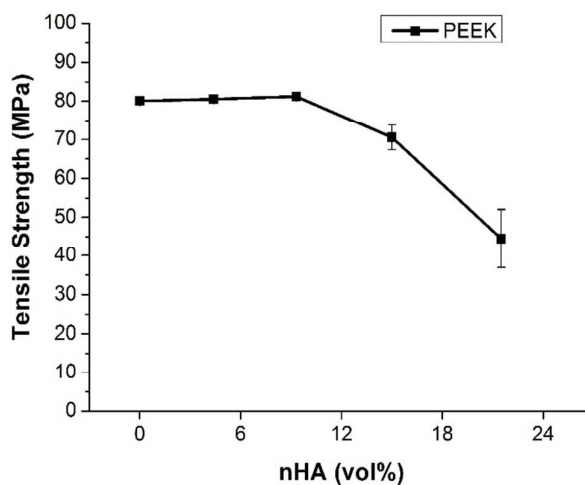
### Mechanical properties

Figure 3 shows the stress-strain curves of pure PEEK, PEEK/nHA and PEEK/nHA-CNF nanocomposites. The nHA additions exhibit beneficial effect in enhancing elastic modulus of PEEK at the expense of tensile ductility. Furthermore, the tensile strength of PEEK/nHA nanocomposites increases slightly with nHA content up to 9.3 vol%, thereafter it decreases with increasing nHA content (Fig. 4). Thus 4.4-9.3 vol% nHA fillers can provide mechanical interlocking with PEEK matrix, thereby reinforcing the polymer matrix. On the contrary, the tensile strength of PEEK/nHA nanocomposites as reported by Wang et al. (Fig. 5) is

lower than that of pure PEEK, and falls rapidly with increasing filler content.<sup>60</sup> Such tensile results indicate poor load-bearing capacity of the nanocomposites. The poor performance of their PEEK/nHA composites is attributed to the use of PEEK powders rather than injection molded PEEK pellets. PEEK powders are unsuitable for injection molding purposes for fabricating nanocomposites. Furthermore, Wang et al. did not employ an extensometer to measure tensile strain of the specimens during tensile testing. As known, Young's modulus of a material is determined from the linear slope of stress-strain curves and not from linear slope of the load-displacement curves. From the Hooke's law, stress varies linearly with elastic modulus and strain in the elastic region.<sup>69</sup> To measure strain, an extensometer is attached to the gauge length of tensile specimen. Therefore, Young's modulus is determined as change in stress divided by change in strain in linear portion of the stress-strain curve.<sup>70</sup> Therefore, elastic modulus of their PEEK and PEEK/nHA composites cannot be determined from the load-displacement curves as shown in Fig. 5.



**Figure 3.** Stress-strain curves of pure PEEK, PEEK/nHA and PEEK/nHA-CNF nanocomposites.



**Figure 4.** Tensile strength versus nHA volume content for PEEK/nHA nanocomposites.

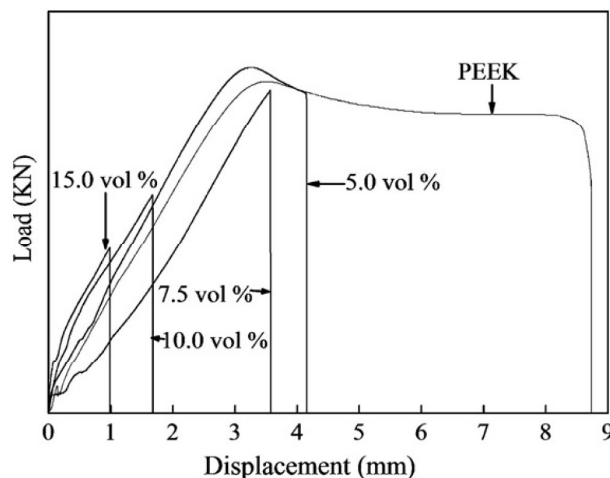


**Figure 5.** Load-displacement curves pure PEEK and PEEK/nHA nanocomposites prepared by mechanical mixing PEEK powders with nHA followed by injection molding.<sup>60</sup>

Figure 6a shows the variation of elastic modulus with nHA content for PEEK/nHA nanocomposites. The elongation vs nHA volume content plot of these nanocomposites is depicted in Fig. 6b. It can be seen that the stiffness of PEEK/nHA nanocomposites increases continuously with increasing nHA content. At 21.5 vol% nHA loading, the stiffness of PEEK/nHA composite reaches 7.85 GPa and exceeds the lower limit of cortical bone with a value of 7 GPa.<sup>58</sup> Despite the high stiffness of PEEK/21.5% nHA nanocomposite,

however, its tensile strength (44.51 MPa) and elongation at break (0.69%) are lower than those of human cortical bone. The tensile stress and fracture strain of cortical bone are 50 MPa and 1%, respectively. The PEEK/21.5% nHA nanocomposite with a tensile strain of 0.69 % is brittle as expected, and unlikely to be used as the material for making bone implants. In this respect, particular attention is paid to tensile behavior of the PEEK/15% nHA nanocomposite with tensile strain of 2.71% and tensile stress of 70.56 MPa because both tensile values are higher than those of cortical bone. The elastic modulus of PEEK/15% nHA nanocomposite is 6.2 GPa (Fig. 6). By adding 1.9 vol% CNF to PEEK/15% nHA nanocomposite, the modulus increases to 6.54 GPa, while the tensile stress and fracture strain also increase to 71.67 MPa and 2.83 %, respectively.

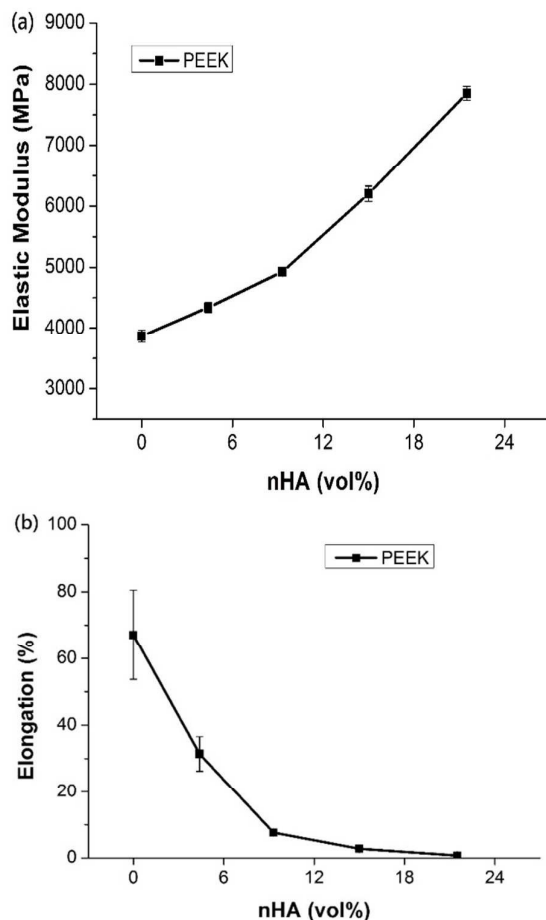


**Figure 6.** (a) Elastic modulus as a function of filler content, and (b) elongation at break vs nHA content for PEEK/nHA nanocomposites.

As aforementioned, metallic implants have many drawbacks for orthopedic applications including corrosion problem, cytotoxicity of metallic ions and stress shielding effect. In the latter case, the extremely large elastic modulus of metallic implants (e.g. Ti-6Al-4Alloy (110 GPa) and Co-Cr alloy (240 GPa)) can lead to stress shielding effect causing bone loss and eventual implant loosening. Stress shielding in femur occurs when some of the loads are taken by the prosthesis and shielded from going to the bone. As a consequence, polymeric materials with low elastic modulus appear to be attractive for use in orthopedics. High-density polyethylene (HDPE) reinforced with 40 vol% nHA particles (HAPEX) have been developed commercially for biomedical applications. The elastic modulus, tensile stress and fracture strain of HAPEX composite are 4.29 GPa, 20.67 MPa and 2.6%, respectively.<sup>71</sup> However, the tensile strength of HAPEX (20.67 MPa) is far below the strength of cortical bone (50 MPa). Thus HAPEX can only be used as non-load bearing biocomposite for maxillofacial surgery, orbital floor prosthesis and middle ear implant.<sup>72</sup> In the present study, PEEK/9.3vol% nHA nanocomposite with favorable mechanical performance, i.e. elastic modulus of 4.92 GPa, tensile stress of 81.23 MPa and fracture strain of 7.62% can replace HAPEX for use in maxillofacial surgery. Moreover, its PEEK matrix with high melting temperature of 343 °C, excellent radiation stability and low moisture absorption provides high level of resistance to sterilization.<sup>20</sup> Therefore, the molecular chains of PEEK do not degrade either during autoclave sterilization or gamma ray radiation treatment. Medical devices must be sterilized in order to prevent the introduction of pathogens into the body. On the contrary, polyethylene is unable to withstand high temperature and pressure conditions during sterilization process. Irradiation of polyethylene results in the scission of molecular chains and the formation of degradation products.<sup>73</sup> In this study, the PEEK/15vol% nHA-1.9vol% CNF bio-nanocomposite with good mechanical performance shows potential for use as the material for load-bearing implants in orthopedics.

### Thermal stability

TGA measurements have been used to provide a substantiate evidence for high thermal stability of PEEK and its nanocomposites (Figure 7). Highly stable PEEK can prevent thermal degradation during sterilization. TGA results of representative specimens are listed in



Table 2. Apparently, PEEK exhibits very high  $T_{10\%}$  and  $T_{30\%}$  decomposition temperatures, demonstrating its high thermal stability. The increase of thermal decomposition temperature is often regarded as an indicator for an improvement in thermal stability. The decomposition temperature of PEEK is considerably higher than that of HDPE (335 °C).<sup>74</sup> Furthermore, the 9.3% nHA addition increases  $T_{30\%}$  of PEEK from 588 to 598 °C. Hybridizing CNF with nHA can further increase  $T_{30\%}$  value of PEEK to 645 °C. The excellent thermal properties of PEEK are attributed to the stability of its aromatic backbone. PEEK consists of bulky molecules that cannot volatilize easily. Therefore, weight loss is not observed until thermal scission products of PEEK volatilized. Thermal degradation of PEEK involves chain scissions of the ether and ketone bonds, giving rise to low molecular volatiles such as diphenyl ether and phenol at high temperatures.<sup>75,76</sup>

From Fig. 7, PEEK decomposes more intensely above 600 °C, resulting in the volatilization of around 45% of the polymer mass. In the presence of 9.3% nHA, large mass loss also occurs above 600 °C, causing volatilization of about 35% of the polymer mass when compared with pure PEEK. The mass loss can be even reduced to 30% by incorporating 15% nHA and 1.9% CNF into PEEK. This result implies that very low CNF loading improves thermal stability of PEEK markedly. Carbon nanofibers generally can be classified as multi-walled carbon nanotubes with larger diameters (less than 500 nm). The beneficial effect of carbonaceous nanomaterials such as carbon nanotubes in enhancing thermal stability of polymers has been reported in the literature. The stabilization effect of carbon nanotubes on the polymer is explained by a barrier effect of the nanotubes, which hinder the diffusion of the degradation products from the bulk of the polymer onto the gas phase.<sup>77</sup>

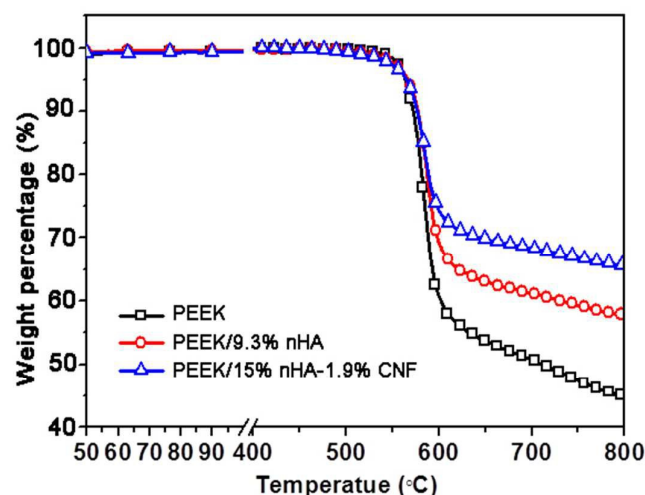


**Figure 7.** TGA curves of pure PEEK, PEEK/9.3vol% nHA and PEEK/15vol% nHA-1.9vol% CNF nanocomposites

**Table 2.** TGA results of PEEK and representative composites

Specimen	$T_{10\%}$ (°C)	$T_{30\%}$ (°C)
PEEK	572	588
PEEK/9.3% nHA	577	598
PEEK/15% nHA-1.9% CNF	577	645

### Cellular adhesion and viability

The adherence of cells to the material surfaces is evaluated through SEM imaging. Figs. 8a-b and 9a-b are the SEM micrographs of PEEK/9.3% nHA and PEEK/15% HA nanocomposites cultured with osteoblasts for 1 and 3 days, respectively. The cells anchor tightly on the surfaces of these composite specimens after cultivation for 1 day. The cells then grow and spread flatly on the surfaces such that many neighbor cells join with each other through cytoplasmic extension after 3 day cultivation. Consequently, entire surface of the PEEK/15% HA nanocomposite is covered with osteoblasts (Fig. 9b). Bioinert PEEK does not promote osteoblastic adhesion and proliferation. The nHA fillers serve as effective sites for the adhesion and growth of osteoblasts. SEM images of cell cultured nanocomposites at day 1 and 3 are presented herein in order to display the difference of cell coverage on the specimen surfaces. Lower cell attachment is seen at day 1 while nearly or full cell coverage is observed at day 3. Above day 3, entire surfaces are covered with osteoblasts.

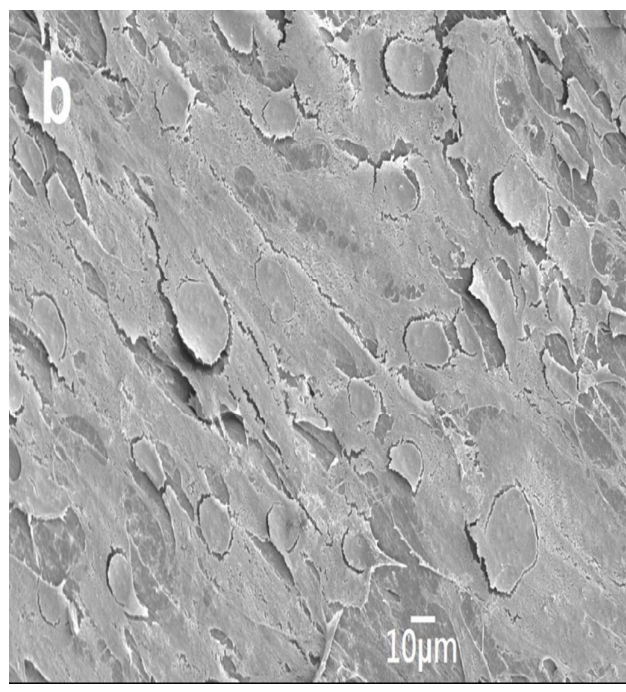
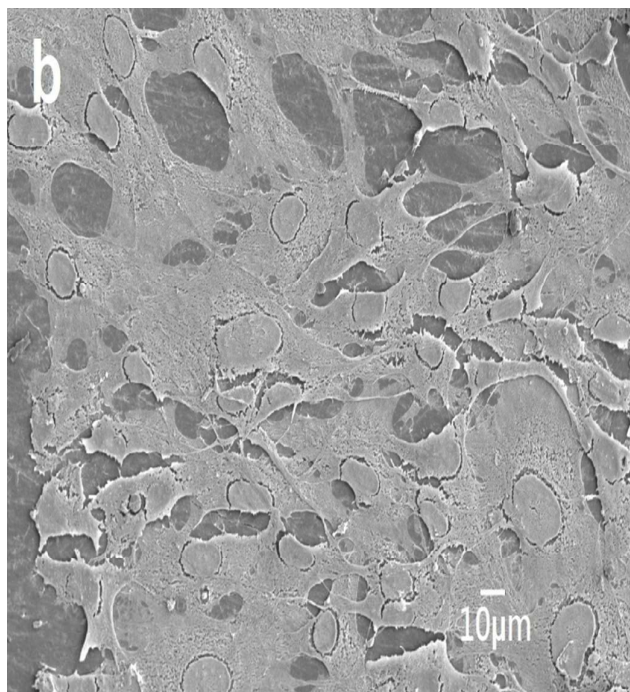
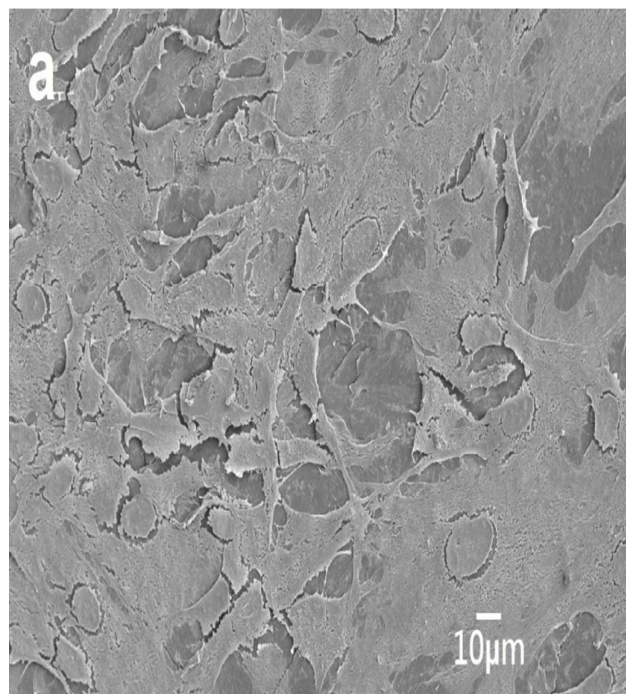
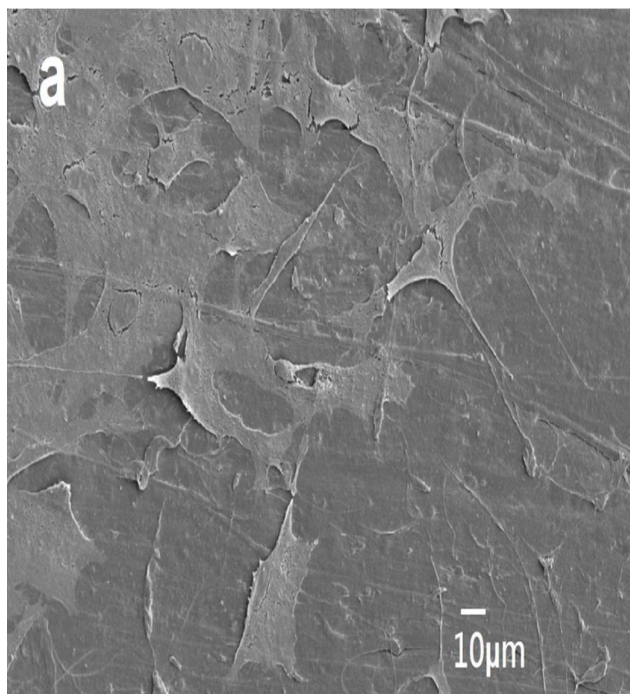


**Figure 8.** SEM micrographs of PEEK/9.3% nHA nanocomposite cultured with osteoblasts for (a) 1 and (b) 3 days.

**Figure 9.** SEM micrographs of PEEK/15% nHA nanocomposite cultured with osteoblasts for (a) 1 and (b) 3 days.

Figure 10 shows the MTT results for PEEK and its nanocomposites. A dramatic increase in cell viability can be observed on PEEK/nHA nanocomposites at every test time period compared to PEEK control. Furthermore, the addition of CNF to PEEK/9.3% nHA and PEEK/15% nHA composites does not impair the viability of osteoblasts. In contrast, a slight increase in cell viability is found for the PEEK/9.3% nHA-1.6% CNF and PEEK/15% nHA-1.9% CNF composites. Comparing with single-walled and multi-walled carbon nanotubes, carbon nanofibers have been reported to have higher cell viability.<sup>64</sup> Price et al. also reported that carbon nanofibers promote osteoblast adhesion.<sup>65</sup> As aforementioned, MTT assay requires additional solubilization step to dissolve color formazan crystals resulting from metabolic activity of mitochondria. Such formazan crystals do not dissolve completely in an organic solvent, particularly in the presence of carbonaceous nanomaterials such as carbon nanotubes.<sup>78</sup> Those undissolved crystals in a solvent can lead to low colorimetric results in the spectrophotometric measurement, resulting in low cell viability. In contrast, WST-1 assay gives water soluble formazan and would not form insoluble clusters like MTT. Therefore, WST-1 assay yields more reliable results for cell viability. Fig. 11 shows the cell viability measured by the WST-1 assay for PEEK-based nanocomposites. It is evident that WST-1 assay gives considerably higher cell viability than MTT assay. From Figs. 10 and 11, MTT and WST-1 tests cover 3, 7 and 10 days. At day 3, the results give low cell viability. Additional 7 and 10 days are needed for testing cell viability in order to achieve higher cell viability. In this respect, the difference in cell viability of each sample becomes more apparent.

It is worth-noting that nanomaterials may induce cytotoxic effect on biological cells. Grabinski et al. indicated that cytotoxicity of carbon materials is dependent on their dimensions.<sup>64</sup> Carbon fiber (10  $\mu\text{m}$  diameter) and CNF (100 nm diameter) did not significantly affect viability of mouse keratinocytes while multiwalled carbon nanotubes (10 nm diameter) reduced cell viability greatly. The cytotoxic action of carbon nanotubes in general is caused by suspending them independently in the cell culture medium. As such, independent carbon nanoparticles can penetrate cell membrane and reside in the cytoplasm.<sup>79,80</sup> Our previous study showed that the polymer matrix of nanocomposites acted as effective material for the

adhesion and encapsulation of CNFs.<sup>81</sup> Therefore, CNFs embedded firmly in the polymer matrix of nanocomposites acting as excellent substrates for the adhesion, growth and viability of osteoblasts.

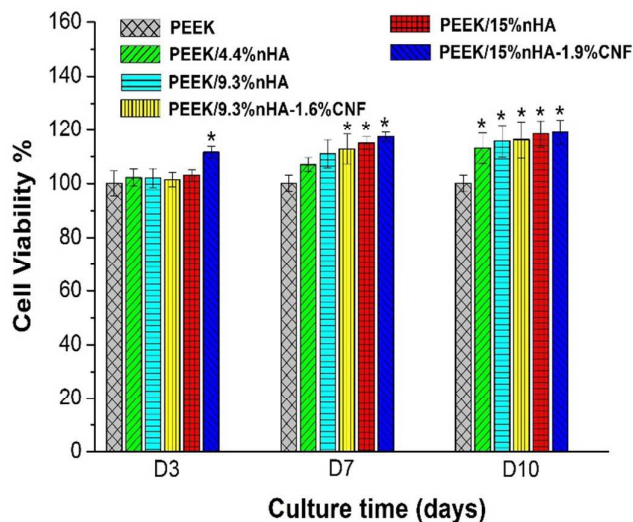


**Figure 10.** MTT assay results showing cell viability of human osteoblasts (Saos-2) grown on PEEK and its nanocomposites for 3, 7 and 10 days. \* represents  $p < 0.05$ .

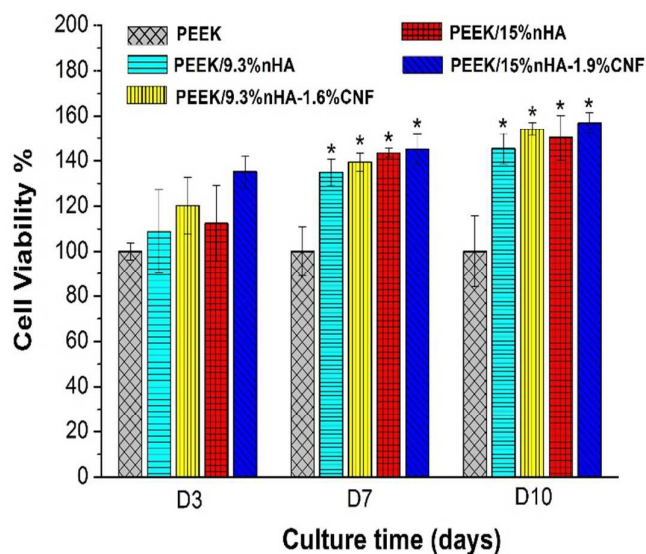


**Figure 11.** WST-1 assay results showing cell viability of human osteoblasts (Saos-2) grown on PEEK and its nanocomposites for 3, 7 and 10 days. \* represents  $p < 0.05$ .

### Alkaline phosphatase activity

Alkaline phosphatase is an important component in hard tissue formation, highly expressed in mineralized tissue cells. Proliferating osteoblasts show alkaline phosphatase activity, and this is greatly enhanced during in vitro bone formation. Alkaline phosphatase catalyzes hydrolysis of phosphate esters in alkaline buffer and produces phenol and inorganic phosphate. Fig. 12 shows the ALP activity of PEEK and its nanocomposites at days 3, 7 and 14. ALP enzymatic assay results reveal good ALP activity level of osteoblasts on the PEEK/nHA composites at day 14. In particular, ALP activity increases with nHA content of the composites. This is because nHA fillers promote osteoblastic cell adhesion and differentiation. In addition, synthetic nHA exhibits excellent osteoconductivity and biocompatibility. As recognized, osteoblastic cell differentiation plays an important role in osteogenesis or bone formation at the earlier stage.<sup>82</sup> ALP is an enzyme produced by cells which participate in bone tissue mineralization through the deposition of minerals on extracellular matrix (ECM) molecules.

From the osteoblastic differentiation model proposed by Stein and Lian,<sup>83</sup> bone cells proliferate greatly up to 7–14 days and then begin to secrete ECM proteins and produce ALP differentiation markers for the matrix mineralization. Upon completion of adhesion and proliferation, osteoblastic differentiation is then initiated to secrete proteins, minerals and collagens for bone tissue mineralization. It is interesting to see that the ALP activity of PEEK/15%nHA nanocomposite can be increased by adding CNF. In previous study, hybridization nHA filler with CNF promotes osteoblastic adhesion and proliferation.<sup>81</sup> CNFs and multiwalled carbon nanotubes have been reported to enhance osteoblastic adhesion and differentiation by promoting protein-material interactions.<sup>65,84,85</sup> Elias et al. demonstrated that osteoblast adhesion, proliferation, alkaline phosphatase activity, and ECM secretion on carbon nanofibers increases with decreasing fiber diameter in the range of 60–200 nm.<sup>84</sup>

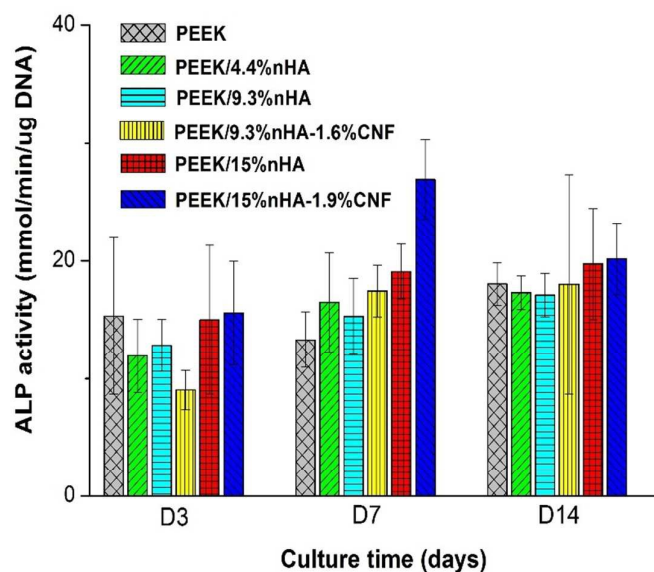


**Figure 12.** ALP activity normalized to DNA content of human osteoblasts (Saos-2) grown on PEEK and its nanocomposites for 3, 7, and 14 days.

### Bioactivity

SBF is a solution that mimics the inorganic ion composition of human plasma. Apatite-forming ability is one of the major mechanisms of chemical bioactivity.<sup>86</sup> By performing SBF immersion, the apatite layer forming ability or bioactivity of our PEEK/nHA and PEEK/nHA-CNF nanocomposites can be assessed. The SBF test is widely used by the researchers to evaluate the capability of test samples to form an apatite layer on their surfaces.<sup>68,86-89</sup> The main difference between SBF and inorganic component of plasma is the carbonate concentration: 4.2 mM in SBF and 27 mM in plasma. The carbonate deficiency in SBF is compensated by a greater concentration of chloride ions, so the electroneutrality of solution is maintained.<sup>68</sup> Figs. 13a is a SEM micrograph showing the morphology of an apatite layer deposited on the surface of PEEK/9.3%nHA nanocomposite after soaking in SBF solution for 21 days. Many globular apatite particles can be seen on the composite surface. X-ray energy dispersive spectrum (EDS) of globular apatite reveals the presence of calcium and phosphorus. The nHA fillers act as nucleation sites for the apatite deposition. The formation mechanism of apatite on the surface of nHA can be attributed to the ion exchange between nHA and the SBF solution.<sup>90,91</sup> The OH<sup>-</sup> and

$\text{PO}_4^{3-}$  groups of the nHA fillers give rise to negatively charged surfaces. Thus  $\text{Ca}^{2+}$  ions in the SBF are attracted towards nHA of the nHA/PEEK nanocomposites. Furthermore, nHA fillers also contain  $\text{Ca}^{2+}$  ions on their surfaces. As more positive charge is built-up,  $\text{PO}_4^{3-}$  ions from the SBF are also attracted to this site, forming calcium phosphate deposits that eventually crystallize into apatite layer.<sup>91</sup> A cross-sectional SEM image of the apatite layer formed on the surface of this nanocomposite is shown in Fig. 13b. Apparently, a dense apatite layer is deposited on the composite surface after soaking for 21 days. Figs. 14a-b are the SEM micrographs showing plan-view and cross-sectional images of the PEEK/15%nHA-1.9%CNF nanocomposite. The plan-view micrograph reveals the presence of more apatite nodules on the surface of this composite with higher nHA content. The nodules then form a compact and continuous layer over the surface. A similar dense apatite layer can be observed on the surface of this nanocomposite (Fig. 14b), demonstrating its good bioactivity.

Comparing with HA fillers of micrometer dimension, the nHA fillers with large surface area favor formation of more apatite nodules as higher  $\text{Ca}^{2+}$  ions and  $\text{PO}_4^{3-}$  groups are concentrated on their surfaces. Moreover, nHA with large surface area provides nucleation sites for apatite nodules. The nucleating effect of apatite nodules increases with nHA content in the nanocomposites. Recently, Yang et al. reported that the incorporation of nHA into polycaprolactone (PCL) facilitates the precipitation of apatite nodules on their surface due to enhanced dissolution of nHA and the subsequent release of  $\text{Ca}^{2+}$  ions, which favors apatite deposition.<sup>92</sup>

A bone-like hydroxyapatite layer generally gives a Ca/P ratio close to 1.65 which is the value reported for bone. The Ca/P ratio values determined from the EDS profiles as shown in Figs. 13a and Fig. 14a are 1.62 and 1.65, respectively. Fig. 15 shows the XRD pattern of mineralized layer on the surface of representative PEEK/15%nHA nanocomposite after immersion in SBF for 21 days. The diffraction peaks of PEEK in the pattern are indexed.<sup>93,94</sup> The small thickness of deposited layer causes the occurrence of PEEK peaks. In addition, nHA peaks can be readily seen in the

pattern. All the nHA planes in the pattern have been indexed in accordance with Joint Committee on Powder Diffraction Standards (JCPDS no. 09-0432) for hydroxyapatite,  $\text{Ca}_{10}(\text{PO}_4)_6(\text{OH})_2$ . From these results, the mineralized layer formed on the composite surface is hydroxyapatite.

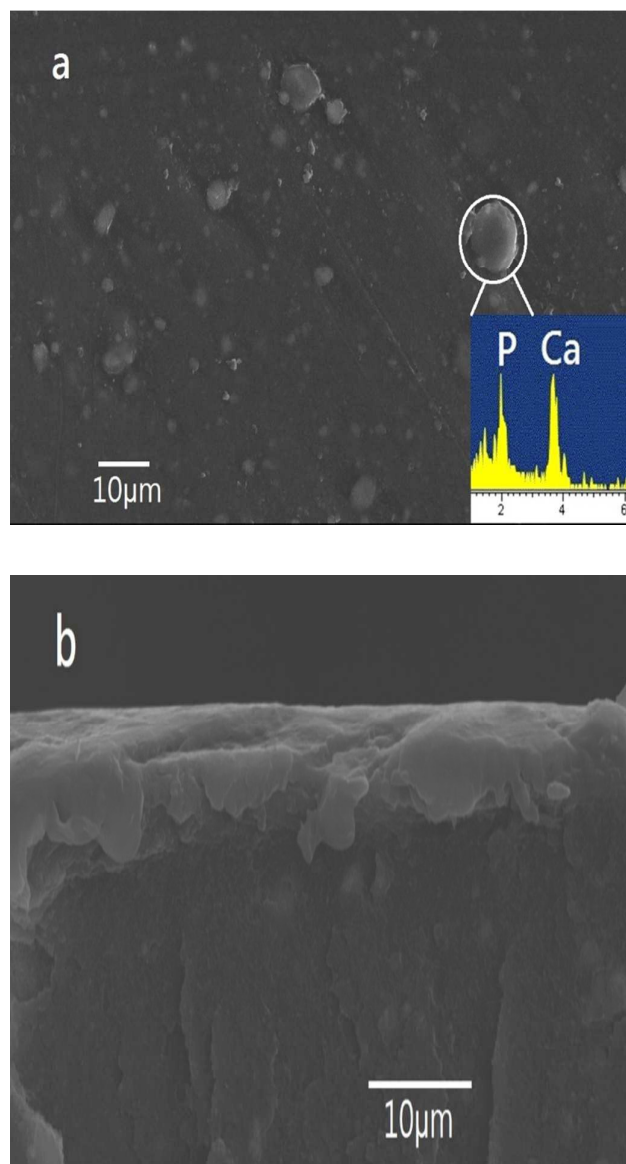


**Figure 13.** (a) Plan-view and (b) cross-sectional SEM micrographs of PEEK/9.3% nHA nanocomposite after soaking in SBF solution for 21 days.

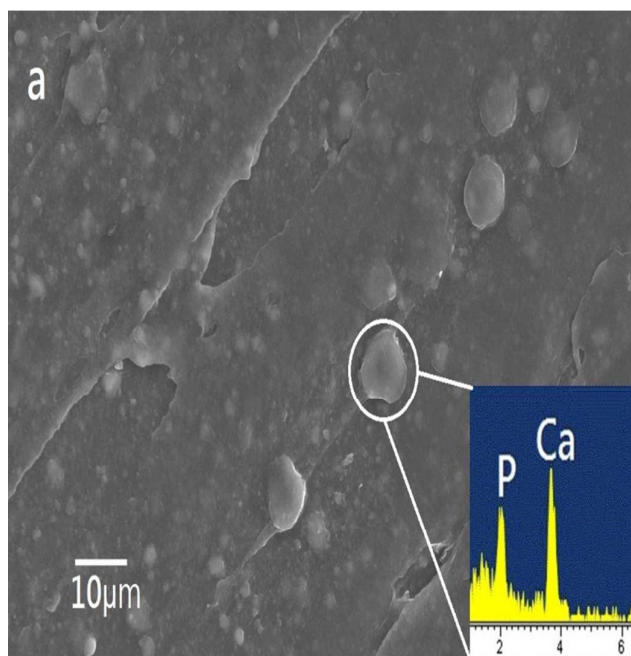


**Figure 14.** (a) Plan-view and (b) cross-sectional SEM images of PEEK/15% nHA-1.9%CNF nanocomposite after soaking in SBF solution for 21 days.

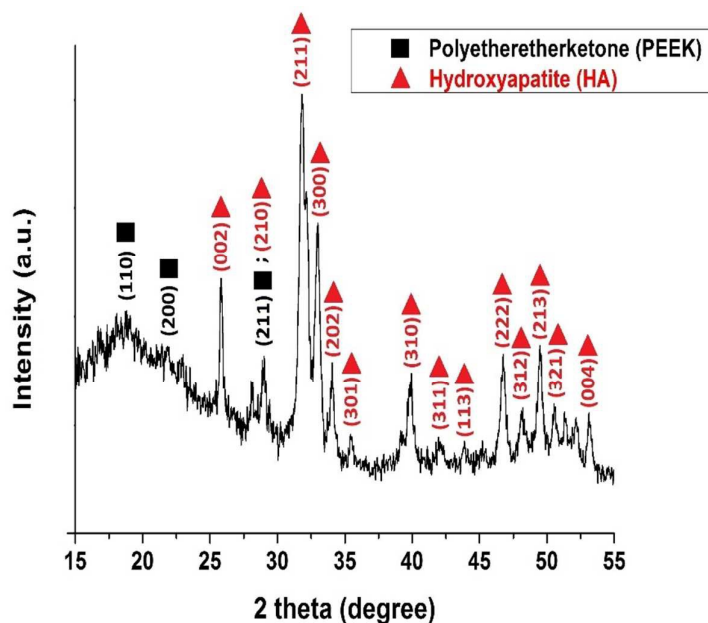


**Figure 15.** XRD pattern of mineralized layer deposited on PEEK/15% nHA nanocomposite after immersion in SBF for 21 days.

### Conclusions

In this article, we presented the preparation, biochemical, mechanical and thermal characterizations of PEEK/nHA and PEEK/nHA-CNF nanocomposites for bone replacements in orthopedics. Our results showed that the PEEK/9.3% nHA nanocomposite with good mechanical, thermal and biological performances can be considered as a biomaterial for use in maxillofacial surgery. This nanocomposite exhibited higher tensile strength than conventional HAPEX composite reinforced with 40vol% HA microparticles. Furthermore, tensile test results revealed that the PEEK/15%nHA-1.9%CNF nanocomposite exhibits comparable tensile properties with human cortical bones. TGA measurements showed that the incorporation of nHA filler or CNF and nHA hybrid fillers into PEEK increases the thermal stability. Hybridization of CNF with nHA fillers was found to increase the  $T_{30\%}$  value of PEEK from 588 °C to 645 °C, and to reduce mass loss effectively at high temperatures. As such, thermal degradation of PEEK hybrid nanocomposite can be avoided during sterilization treatment. Accordingly, PEEK/15% nHA-1.9%CNF nanocomposite shows high potential for use as a biomaterial for load-bearing implants.

MTT and WST-1 results demonstrated that cell viability of osteoblasts increases with increasing nHA content in the PEEK/nHA nanocomposites. In addition, PEEK/nHA nanocomposite with high nHA content (i.e. 15%) exhibited higher ALP activity compared to pure PEEK. The presence of the nHA mineral phase enhanced ALP activity, an early marker of bone formation. Moreover, CNF addition further increased ALP activity of the PEEK/15% nHA nanocomposite.

### Acknowledgement

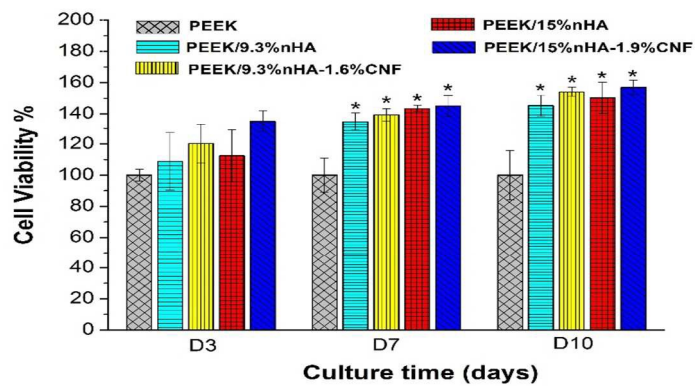
This work is supported by a Strategic Research Grant (Project No. 7004384), City University of Hong Kong and Shenzhen Science and Technology Project Grant (JCYJ20150630145302228), China.

### References

- C. M. Aldwin and D. F. Gilmer, *Health, Illness, and Optimal Aging: Biological and Psychosocial Perspectives*, Springer, New York, 2013.
- T. Denning and A. Thomas, *Old Age Psychiatry*, 2nd Ed., Oxford University Press, Oxford, 2013.
- A. Oryan, S. Alidadi, A. Moshiri and N. Maffulli, *J. Orthop. Surg. Res.*, 2014, **9**, 18.
- M. Navarro, A. Michiardi, O. Castan and J. A. Planell, *J. R. Soc. Interface*, 2008, **5**, 1137-1158.
- J. J. Jacobs, J. L. Gilbert and R. M. Urban, *J Bone Joint Surg. Am.* 1998, **80A**, 268-282.
- N. Hallab, K. Meritt and J. J. Jacobs, *J Bone Joint Surg. Am.* 2001, **83 A**, 428-436.
- Y. Okazaki and E. Gato, *Biomaterials*, 2005, **26**, 11-21.
- B. Scharf, C. C. Clement, V. Zolla, G. Perino, B. Yan, S. G. Elci, E. Purdue, S. Goldring, F. Macaluso, N. Cobelli, R. W. Vachet and L. Santambrogio, *Sci. Rep.*, 2014, **4**, 5729.
- V. S. Challa, S. Mali and R. D. K. Misra, *J. Biomed. Mater. Res. A*, 2013, **101**, 2083-2089.
- S. C. Tjong and E. B. Yeager, *J. Electrochem. Soc.*, 1981, **128**, 2251-2254.
- S. C. Tjong, R. W. Hoffman and E. B. Yeager, *J. Electrochem. Soc.*, 1982, **129**, 1662-1668.
- N. Cobelli, B. Scharf, G. M. Crisi, J. Hardin and L. Santambrogio, *Nature Rev. Rheumatology*, 2011, **7**, 600-608.
- J. Pajarinen, T.H. Lin, T. Sato, Z. Yao and S. B. Goodman, *J. Mater. Chem. B*, 2014, **2**, 7094-7108.
- S. C. Tjong and Y. Z. Meng, *Eur. Polym. J.*, 2000, **36**, 123-129.
- Y. Z. Meng, S. C. Tjong, A. S. Hay and S. J. Wang, *J. Polym. Sci. Part A-Polym. Chem.*, 2001, **39**, 3218-3226.
- X. H. Li, S. C. Tjong, Y. Z. Meng and Q. Zhu, *J. Polym. Sci. Part B- Polym. Phys.*, 2003, **41**, 1806-1813.
- Y. Z. Meng and S. C. Tjong, *Polymer*, 1998, **39**, 99-107.
- Y. Z. Meng, A. S. Hay, X. G. Jian and S. C. Tjong, *J. Appl. Polym. Sci.*, 1998, **68**, 137-143.
- L. C. Du, Y. Z. Meng, S. J. Wang and S. C. Tjong, *J. Appl. Polym. Sci.*, 2004, **92**, 1840-1846.
- A. M. Díez-Pascual, M. Naffakh, C. Marco, G. Ellis, M.A. Gómez-Fatou, *Prog. Mater. Sci.*, 2012, **57**, 1106-1190.
- S. M. Kurtz and J. N. Devine, *Biomaterials*, 2007, **28**, 4845-4869.
- E. L. Steinberg, E. Rath, A. Slaifer, O. Chechik, E. Maman and M. Salai, *J. Mech. Behav. Biomed. Mater.*, 2013, **17**, 221-228.
- R. K. Ponnappan, H. Serhan, B. Zarda, R. Patel, T. Albert and A. R. Vaccaro, *Spine J.*, 2009, **9**, 263-267.
- M. R. Abdullah, A. Goharian, M. R. Kadir, M. U. Wahit, *J. Biomed. Mater. Res. A*, 2015, **103**, 3689-3702.
- E. Alonso-Rodriguez, J.L. Cebrián, M.J. Nieto, J. L. Del Castillo, J. Hernández-Godoy and M. Burgueno, *J. Craniomaxillofac Surg.*, 2015, **43**, 1232-1238.
- R. Ma, S. Tang, H. Tan, J. Qian, W. Lin, Y. Wang, C. Liu, J. Wei and T. Tang, *ACS Appl. Mater. Interfaces*, 2014, **6**, 12214-12225.
- Y. Zhao, H. M. Wong, W. Wang, P. Li, Z. Xu, E. Y. Chong, C. Yan, K. W. Yeung and P. K. Chu, *Biomaterials*, 2013, **34**, 9264-9277.
- Z. Novotna, A. Reznickova, S. Rimpelova, M. Vesely, Z. Kolska and V. Svorcik, *RSC Adv.*, 2015, **5**, 41428-41436.
- A. A. John, A. P. Subramanian, M. V. Vellayappan, A. Balaji, S. K. Jaganathan, H. Mohandas, T. Paramalinggam, E. Supriyanto and M. Yusof, *RSC Adv.*, 2015, **5**, 39232-39244.
- R. K. Roeder, M. M. Sproul and C. H. Turner, *J. Biomed. Mater. Res.*, 2003, **67**, 801-812.
- G. L. Converse, W. M. Yue, R. K. Roeder, *Biomaterials*, 2007, **28**, 927-935.
- S. M. Tang, P. Cheang, M. S. Abu Bakar, K. A. Khor, K. Liao, *Int. J. Fatigue*, 2004, **26**, 49-57.
- M. S. Abu Bakar, M. H. Cheng, S. M. Tang, S. C. Yu, K. Liao, C.T. Tan, K. A. Khor, P. Cheang, *Biomaterials*, 2003, **24**, 2245-2250.
- J. Z. Liang, R. K. Y. Li and S. C. Tjong, *Polymer Compos.*, 1999, **20**, 413-422.
- K. L. Fung, R. K. Y. Li and S. C. Tjong, *J. Appl. Polym. Sci.*, 2002, **85**, 169-176.
- Y. Z. Meng and S. C. Tjong, *Polymer*, 1998, **39**, 99-107.
- X.L. Xie, B.G. Li, Z.R. Pan, R.K.Y. Li and S.C. Tjong, *J. Appl. Polym. Sci.*, 2001, **80**, 2105-2112.
- S. C. Tjong, *Carbon Nanotube Reinforced Composites: Metal and Ceramic Matrices*, Wiley-VCH, Weinheim, Germany, 2009, 1-228.
- S. C. Tjong and Y. Z. Meng, *Polymer*, 1997, **38**, 4609-4615.
- M. Colilla, B. González and M. Vallet-Regí, *Biomater. Sci.*, 2013, **1**, 114-134.
- P. A. Tran, L. Sarin, R. H. Hurt and T. J. Webster, *J. Mater. Chem.*, 2009, **19**, 2653-2659.

42. V. B. Damodaran, D. Bhatnagar, V. Leszczak and K.C. Popa, *RSC Adv.*, 2015, **5**, 37149-37171.
43. Z. J. Han, A. E. Rider, M. Ishaq, S. Kumar, A. Kondyurin, M. M. Bilek, I. Levchenko and K. Ostrikov, *RSC Adv.*, 2013, **3**, 11058-11072.
44. K. Kavitha, W. Chunyan, D. Navaneethan, V. Rajendran, S. Valiyaveetil and A. Vinoth, *RSC Adv.*, 2013, **4**, 43951-43961.
45. J. Zhang and T. J. Webster, *Nano Today* 2009, **4**, 66-80.
46. G. Suresh Kumar, L. Sathish, R. Govindan and E. K. Girija, *RSC Adv.*, 2014, **5**, 39544-39548.
47. H. Zhou and J. Lee, *Acta Biomater.*, 2011, **7**, 2769-2781.
48. S. K. Natarajan and S. Selvaraj, *RSC Adv.*, 2014, **4**, 14328-14334.
49. Z. Tao, *RSC Adv.*, 2014, **4**, 18961-18980
50. M. Ghadiri, W. Chrzanowski and R. Rohanizadeh, *RSC Adv.*, 2015, **5**, 29467-29481
51. M. Peran, A. A. Garcia, E. Lopez-Ruiz, G. Jimenez and J. A. Marchal, *Materials*, 2013, **6**, 1333-1359.
52. F. Mohandes and M. Salavati-Niasari, *RSC Adv.*, 2014, **4**, 25993-26001.
53. M.R. Rogel, H. Qiu and G.A. Ameer, *J. Mater. Chem.*, 2008, **18**, 4233-4241.
54. S. C. Tjong and S. P. Bao, *Compos. Sci. Technol.*, 2007, **67**, 314-323.
55. Y. C. Li, S. C. Tjong and R. K. Y. Li, *Synth. Met.*, 2010, **160**, 1912-1919.
56. S. C. Tjong and G. D. Liang, *Mater. Chem. Phys.* 2006, **100**, 1-5.
57. L. He and S. C. Tjong, *RSC Adv.*, 2015, **5**, 15070-15076.
58. W. Bonfield, M. Wang and K. E. Tanner, *Acta Mater.*, 1998, **46**, 2509-2518.
59. K. Li, C. Y. Yuen, K. W. Yeung and S. C. Tjong, *Adv. Eng. Mater.*, 2012, **14**, B155-B165.
60. C. Z. Liao, H. M. Wong, K. W. K. Yeung and S. C. Tjong, *Mater. Sci. Eng. C- Mater. Biol. Appl.*, 2013, **33**, 1380-1388.
61. J. Venkatesan and S. K. Kim, *J. Biomed. Nanotechnol.*, 2014, **10**, 3124-3140.
62. F. Sun, H. Zhou and J. Lee, *Acta Biomater.*, 2011, **7**, 3813-3829.
63. L. Wang, L. Weng, S. Song, Z. Zhang, S. Tian and R. Ma, *Mater. Sci. Eng. A*, 2011, **528**, 3689-3696.
64. C. Grabinski, S. Hussain, K. Lafdi, L. Braydich-Stolle and J. Schlager, *Carbon*, 2007, **45**, 2828-2835.
65. P. L. Price, M. Waid, K. Haberstroh and T. J. Webster, *Biomaterials*, 2003, **24**, 1877-1887.
66. J. Sandler, P. Werner, M. S. Shaffer, V. Demchuk, V. Altstad and A. H. Windle, *Composites Part A*, 2002, **33**, 1033 - 1039.
67. T. Kokubo and H. Takadama, *Biomaterials*, 2006, **27**, 2907-2915.
68. A. J. Salinas and M. Vallet-Regi, *RSC Adv.*, 2013, **3**, 11116-11131.
69. W. D. Callister and D. G. Rethwisch, *Materials Science and Engineering: An Introduction*, 9th Ed., John Wiley, New York, 2013.
70. G. Tetteh, A. S. Khan, R. M. Delaine-Smith, G. C. Reilly and I. U. Rehman, *J. Mech. Behav. Biomed. Mater.*, 2014, **39**, 95-110.
71. L. D. Silvio, M. J. Dalby and W. Bonfield, *Biomaterials*, 2002, **23**, 101-107.
72. R.N. Downes, S.Vardy, K. E. Tanner and W. Bonfield, *Bioceramics*, 1991, **4**, 239 -246.
73. B. Gewert, M. M. Plassmann and M. MacLeod, *Environ. Sci.: Processes Impacts*, 2015, **17**, 1513-1521.
74. C. J. Hilado, *Flammability Handbook For Plastics*. Fifth Edition. Chapter 2, 1998, Technomic Publishing Company Inc, Pennsylvania, USA.
75. L. H. Perng, C. J. Tsai and Y. C. Ling, *Polymer*, 1999, **40**, 7321-7329.
76. P. Patel, T. R. Hull, R.W. McCabe, D. Flath, J. Grasmeder, and M. Percy, *Polym. Degr. Stab.* 2010, **95**, 709-718.
77. D. Bikiaris, A. Vassiliou, K. Chrissafis, K.M. Paraskevopoulos, A. Jannakoudakis and A. Docoslis, *Polym. Degr. Stab.* 2008, **93**, 952-967.
78. J. M. Worle-Knirsch, K. Pulskamp, and H. F. Krug, *Nano Lett.*, 2006, **6**, 1261-1268.
79. J. Muller, H. Huaux and D. Lison, *Carbon* 2006, **44**, 1048-1056.
80. A. Porter, M. Gass, K. Muller, J. N. Skepper, P. A. Midgley and M. Welland, *Nat. Nanotechnol.* 2007, **2**, 713-717.
81. C. Z. Liao, H. M. Wong, K. W. K. Yeung and S. C. Tjong, *Int. J. Nanomed.*, 2014, **9**, 1299-1310.
82. A. K. Gaharwar, S. M. Mihaila, A. Swami, A. Patel. S. Sant and R. L. Reis, *Adv. Mater.* 2013, **25**, 3329-36.
83. G. S. Stein and J. B. Lian, *Endocrine Rev.*, 1993, **14**, 424-442.
84. E. K. Elias, P. L. Price and T. J. Webster, *Biomaterials*, 2002, **23**, 3279-3287
85. X. Li, H. Gao, M. Uo, Y. Sato, T. Akasaka, Q. Feng, F. Cui, X. Liu and F. Watari, *J. Biomed. Mater. Res. A.*, 2009, **91**, 132-139.
86. A. B. Zadpoor, *Mater. Sci. Eng. C*, 2014, **35**, 134-143.
87. J. Ni and M. Wang, *Mater. Sci. Eng. C- Mater. Biol. Appl.*, 2002, **20**, 101-109.
88. W. Chrzanowski, W. J. Yeow, R. Rohanizadeha and F. Dehghani, *RSC Adv.*, 2012, **2**, 9214-9223.
89. T. Akasaka, F. Watari, Y. Sato and K. Tohji, *Mater. Sci. Eng. C- Mater. Biol. Appl.*, 2006, **26**, 675-678.
90. H. M. Kim, T. Himeno, T. Kokubo and T. Nakamura, *Biomaterials*, 2005, **26**, 4366-4373.
91. N. M. Alves, I. B. Leonor, H. S. Azevedo, R. L. Reis and J. F. Mano, *J. Mater. Chem.*, 2010, **20**, 2911-2921.
92. F. Yang, S. K. Both, X. Yang, X. F. Walboomers and J. A. Jansen, *Acta Biomater.*, 2009, **5**, 3295-3304.
93. T. Liu, S. Wang, Z. Mo, H. Zhang, *J. Appl. Polym. Sci.*, 1999, **73**, 237-243
94. J.N. Hay, J.I. Langford, J.R. Lloyd, *Polymer*, 1989, **30**, 489-493





WST-1 assay shows that PEEK/15vol% nHA-1.9vol% CNF hybrid composite with excellent biocompatibility